

Hybrid Control of Flowrate in Microextrusion-Based Direct-Write Additive Manufacturing

Ali Asghari Adib[®], *Graduate Student Member, IEEE*, and David J. Hoelzle[®], *Member, IEEE*

Abstract—Flowrate control has been a continuous challenge in Direct-Write Additive Manufacturing (DW AM) due to capacitive energy storage in the system and the lack of suitable flowrate sensors at the microscale, resulting in poor dimensional control of material addition. While a pressure sensor can be used for pressure-based feedback control, the system will become marginally stable if the material loses contact with the pressure sensor, and thus feedback is lost. In this letter, we design and implement a pressure-based hybrid controller with a state-dependent switching strategy that eliminates the stability problem due to a loss of pressure feedback, and thus enables the real time, stable control of flowrate in DW AM. The stability of the hybrid controller is assessed using phase portraits and Multiple Lyapunov-like Functions. The hybrid dynamical model and the hybrid controller are experimentally implemented and validated. Stability results indicate that the hybrid controller resolved the marginal stability issue, and is stable in the sense of Lyapunov. Moreover, the hybrid control scheme implementation in the case study demonstrated that the shape fidelity of the parts is appreciably enhanced compared to the open loop control case.

Index Terms—Switched systems, stability of hybrid systems, hybrid control, controls implementation, direct-write additive manufacturing.

I. INTRODUCTION

IRECT-WRITE (DW) additive manufacturing (AM) enables the three dimensional (3D) fabrication of parts [1] for various industrial and biomedical applications [2], [3] by the controlled, layer-by-layer, extrusion of build material (ink) filaments. Micro Robotic Deposition (μ RD) system is an example of a DW AM systems (Fig. 1a) widely used by researchers [4], [5]. Despite the vast use of DW

Manuscript received September 14, 2020; revised December 10, 2020; accepted December 22, 2020. Date of publication January 8, 2021; date of current version June 23, 2021. This work was supported in part by NSF under Grant CMMI-1708819 and Grant IIP-1919204. Recommended by Senior Editor J. Daafouz. (Corresponding author: David J. Hoelzle.)

The authors are with the Department of Mechanical Engineering, Ohio State University, Columbus, OH 43210 USA (e-mail: asghariadib.1@osu.edu; hoelzle.1@osu.edu).

Digital Object Identifier 10.1109/LCSYS.2021.3049897

trol that are due to the capacitive energy storage in the system resulting in transient behavior with a slow time constant [5]. As shown in Fig. 1b [5], in an open loop controlled DW AM, there is a lack of ink deposition at the start of printing as the capacitive energy is being stored, and there is unwanted excess ink deposition after the stop of printing, as the capacitive energy is dissipated. Although there is a lack of suitable flowrate sensors for DW AM, a pressure sensor can be used (Fig. 1a) as surrogate for a flowrate sensor as there is a welldefined, static relationship between flowrate and pressure with the fluids used in DW [6]. However, aggressive stopping of flowrate requires quick retraction of material, which may cause the material to lose contact with the pressure sensor, which will result in the loss of feedback signal, and the system will be marginally stable (Fig. 1d). Given this distinct change in feedback, hybrid system theories [7], [8] can be utilized for modeling and control of continuous dynamics and discrete switching events in the system. We define the DW system as having a volumetric flowrate input, Q_{in} (m^3/s), that is imposed by the plunger, volumetric flowrate output, Q_{out} (m^3/s), which defines the material added to the structure, ink gauge pressure, P(kPa), as the state, and ink leading edge position a(mm), defined as the distance of the material tip from the nozzle tip, as an augmented state. State a is simply the scaled integral of the output flowrate (Q_{out}) to predict the location of ink leading edge in the nozzle (Fig. 1e). The model consists of four modes with their associated partitions in the state space (Fig. 1c and e): Mode 1 occurs when the ink is being extruded or is idle at the tip of the nozzle, and ink leading edge is not being calculated (a = 0); Mode 2 occurs when there is a negative pressure, thus negative flowrate, and the ink is retracting up the nozzle, where the calculation of ink leading edge position, a, is active; Mode 3 occurs when the leading edge position has passed a user-defined position, a_d , and Mode 4, occurs when a passes the location of the sensor (a_s) and the ink will not contact the sensor, leading to the loss of the pressure feedback signal. Mode 3 is introduced into the system in order to switch controller action to prevent the material from losing contact with the sensor. The state based switching criteria was discussed in detail previously [6]. The switching criteria for

AM, there are still challenges associated with ink flowrate con-

2475-1456 © 2021 IEEE. Personal use is permitted, but republication/redistribution requires IEEE permission. See https://www.ieee.org/publications/rights/index.html for more information.

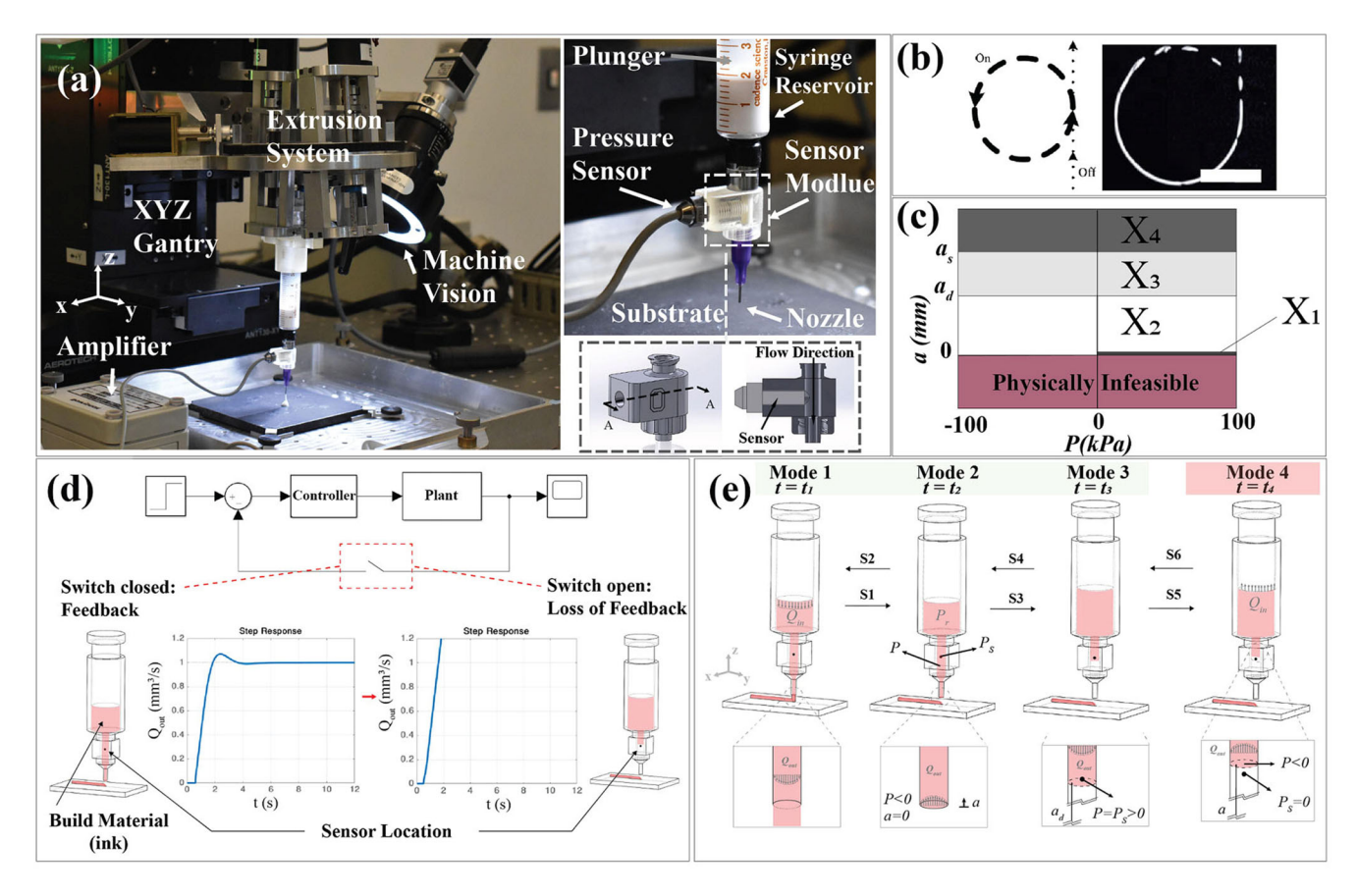


Fig. 1. Direct-Write Additive Manufacturing (DW AM) challenges and pressure based hybrid control as a solution. Micro robotic deposition (μ RD) system equipped with a pressure sensor module. Sensor module 3D view and cross-section A-A is shown in the inset (a). Open loop control yields a lack of ink at the start and an excess of ink at the stop of the flowrate (obtained from our previous work [5], scale bar denotes 5 mm) (b). The partitions of state space with respect to the modes (c). Hypothetical response of the feedback system under feedback and loss of feedback signal. The system is marginally stable when feedback is lost (d). The hybrid model representation of the system (modified from [6]) (e).

transitioning from Mode 1 to Mode 2 (S1), and from Mode 2 to Mode 1 (S2) are

S1:
$$a = 0$$
 and $P < 0$

S2:
$$a = 0$$
 and $P \ge 0$.

The switching criteria for transitioning from Mode 2 to Mode 3 is

S3:
$$a = -\int \frac{Q_{out}}{A} dt \ge a_d$$
,

where A is the nozzle area. The system will transition from Mode 3 back to 2 when

S4:
$$a = -\int \frac{Q_{out}}{A} dt < a_d$$
.

Mode 4 occurs when $a > a_s$ (S5), where a_s is the ink leading edge position at which the feedback signal is lost $y = P_s = 0$. The system will switch back to Mode 3 when $a < a_s$ (S6).

Here, we design and analyze the stability of a hybrid pressure feedback controller that controls the flowrate in DW AM. The designed controller is also implemented experimentally and demonstrates that it resolves the marginal stability issue in a normal pressure feedback controller in DW AM, when material loses contact with sensor. Model development and validation are reported in Sections II and III. The hybrid controller design, stability analysis using phase portraits applied

to the nonlinear model and multiple Lyapunov-like functions applied to the linearized model, and experimental implementation are discussed in Section IV. A case study of printing with and without the designed control scheme is presented in Section IV, demonstrating the successful performance of the controller. Finally, concluding remarks are presented in Section V.

II. MODEL DEVELOPMENT

A. Assumptions

1) Continuous Dynamics:

- **A1:** The ink is a non-Newtonian yield-pseudoplastic fluid (YPF) and thus is modeled by the Herschel-Bulkley equation (Eq. (2)).
- **A2-A4:** These assumptions are the same as assumptions A2-A4 in our previous work [6].

2) Discrete Dynamics:

- A5: Once the ink has left the nozzle it will not return to the nozzle.
- **A6:** Sensor module and nozzle are combined as one unit with the sensor acting as a point probe [6].

B. Continuous Microextrusion Dynamics

The system is composed of a reservoir, sensor module section and a nozzle (Fig. 1a). Since the nozzle section dominates

the effect on steady state pressure, the governing equations for the continuous flow through the microextrusion system was derived for a simplified geometric model consisting only a nozzle section with an effective length and a reservoir.

$$\dot{P} = \frac{\beta}{V_r} (Q_{in} - Q_{out}), \tag{1}$$

$$Q_{out} = \begin{cases} \pi R^3 n \left(\frac{-\tau_w}{m}\right)^{1/n} (1 - \phi)^{(n+1/n)} \left[\frac{(1-\phi)^2}{3n+1} + \frac{2\phi(1-\phi)}{2n+1} + \frac{\phi^2}{n+1}\right] \\ \text{for } \phi \le 1 \\ 0 \\ \text{for } \phi > 1. \end{cases}$$

where β is bulk modulus and V_r is reservoir volume. The output volumetric flowrate, Q_{out} , in Eq. (1), can be expressed by Eq. (2), where R is the nozzle radius, m is the fluid consistency index, n is the flow behavior index, $\tau_w = \frac{P}{L} \frac{R}{2}$ is the wall shear stress, L is the effective nozzle length, and $\phi = \frac{\tau_0}{\tau_w}$, where τ_0 is the yield stress [9].

C. Hybrid System

The discrete dynamics and switching criteria were fully discussed formerly [6], and in Section I. The nonlinear hybrid system encompassing both continuous and discrete dynamics of the system can be represented by the following equations [6]:

$$\dot{x} = f(x, u, q)$$
$$y = h(x, q)$$

where the state $x \in \mathbb{R}^2$, and \mathbb{R}^2 is the continuous state space, $u \in \mathbb{R}, f \colon \mathcal{Q} \times \mathbb{R} \times \mathbb{R}^2 \to \mathbb{R}^2$ is the vector field, where \mathcal{Q} is the set of discrete states, $y \in \mathbb{R}$ is the output, and $h \colon \mathcal{Q} \times \mathbb{R}^2 \to \mathbb{R}$ is the output mapping [10], [11]. Modes are denoted by $q \in \mathcal{Q}$, of which there are four discrete modes. The nonlinear (NL) model was linearized about $\bar{x} = [\bar{P} \quad \bar{a}]$ and $\bar{u} = \bar{Q}_{in}$ [12], and the resulting state space hybrid representation with state-based switching criteria as described in Section I is

$$\begin{bmatrix} \dot{P} \\ \dot{a} \end{bmatrix} = \begin{bmatrix} A_{11} & 0 \\ A_{21,q} & 0 \end{bmatrix} \begin{bmatrix} P \\ a \end{bmatrix} + \begin{bmatrix} B & -A\bar{x} \end{bmatrix} \begin{bmatrix} u_q - \bar{Q}_{in} \\ 1 \end{bmatrix},$$

$$y = \begin{bmatrix} c_q & 0 \end{bmatrix} \begin{bmatrix} P \\ a \end{bmatrix}$$

$$A_{21,q} = \begin{cases} 0 & q = 1 \\ A_{21} & q = 2 \\ A_{21} & q = 3 \\ A_{21} & q = 4 \end{cases} \quad c_q = \begin{cases} 1 & q = 1 \\ 1 & q = 2 \\ 1 & q = 3 \\ 0 & q = 4. \end{cases}$$

III. MODEL VALIDATION

For experimental investigations, a custom-built μ RD (Fig. 1a) was used as the DW AM system with a 0.510 mm inner diameter nozzle and a stage speed of 5 mm/s. An Endevco model 8530-C pressure transducers (PCB Piezotronics, NC) was used to monitor pressure during printing. A sensor module was placed between the syringe and the nozzle (Fig. 1a) with a through threaded hole that allows the pressure sensor to be oriented perpendicular to the fluid channel. A model UV-10 in-line amplifier (#060-6827-04, Honeywell, NC) was used to amplify the mV output of the pressure transducer 100 times. A Quanser QPIDe data

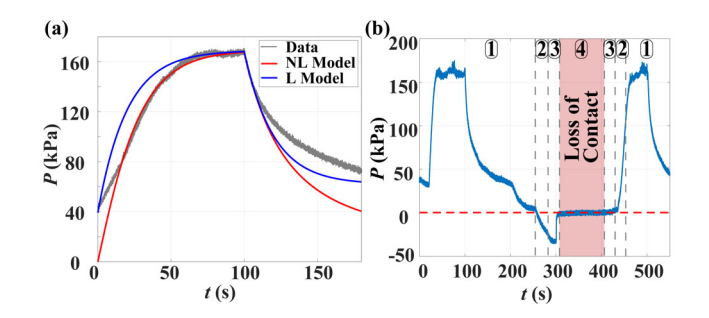


Fig. 2. Nonlinear (NL) and linear (L) model responses validation (a). Validation of different modes in the experimental DW AM setup (b).

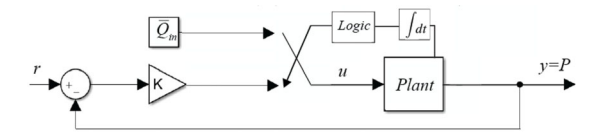


Fig. 3. Multi-controller block diagram.

acquisition (DAQ) system was used to read the analog output of the sensor. The pressure response for the experimental system is compared to the nonlinear and linearized models for a pulse Q_{in} input (Fig. 2a). The percent normalized rootmean-square error (% NRMSE) for the nonlinear model and linearized model was 13% and 10%, respectively. The presence of the four hypothesized modes is validated with a Q_{in} input designed to cause the system to progress through all four modes and shown in Fig. 2b.

IV. HYBRID CONTROL DESIGN AND IMPLEMENTATION A. Multi-Controller Design

For Mode 1 and Mode 2, in which we have feedback, an output feedback control law is designed for a desired time constant of 0.25~s, to yield a suitable response for printing at stage speed of 5~mm/s. The state space representation for the linearized model (Section II) is converted to a transfer function, and after pole zero cancellation associated with the augmented state, a, the time constant of the first order transfer function with pole associated with the state, P, in the left hand plane, was utilized to tune the controller gain K, and obtain an output feedback law of the form

$$u_q = K(r - y) \quad q \in \{1, 2\}$$

where u_q is the control input, q denotes the mode of the system, $K = 7.69 \times 10^{-13}$ is the controller gain, and $r \in \mathbb{R}$ is the reference pressure.

For Mode 3, which is designed to prevent the system from entering Mode 4, and Mode 4 in which the pressure feedback signal is lost (y = 0), a constant predefined open loop control input of the form

$$u_q = \bar{Q}_{in} \quad q \in \{3, 4\}$$

is designed to force a positive flowrate Q_{out} to make sure there is not a loss of contact between the ink and the pressure sensor. Here we use $\bar{Q}_{in}=1.02\times 10^{-9}~m^3/s$. The multi-controller block diagram is demonstrated in Fig. 3. The controller switches according to the state dependent criteria discussed in Section I.

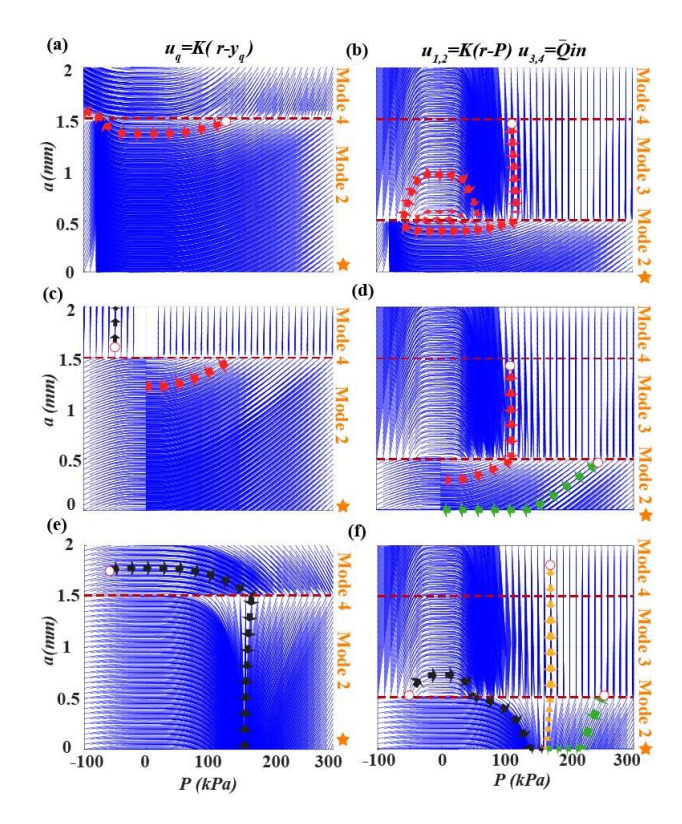
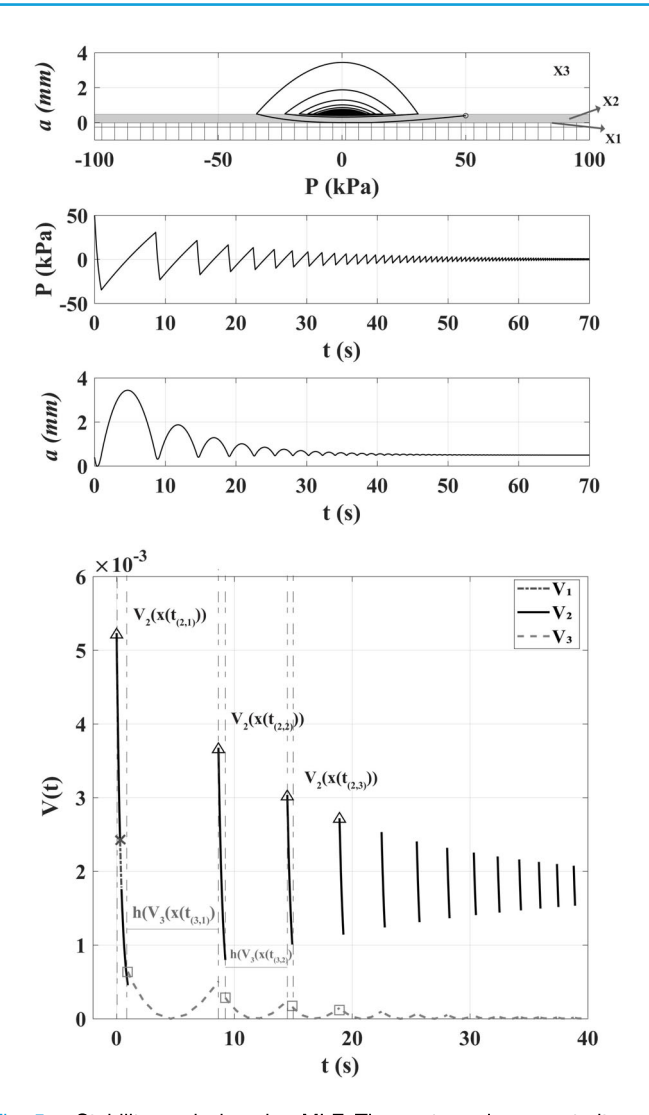


Fig. 4. Phase portraits of the system regulating r = -P with output feedback (a) and with hybrid control (b), r=0 with output feedback (c) and with hybrid control (d), and $r=\bar{P}$ with output feedback (e) and with hybrid control (f). Star sign denotes Mode 1. Arrows from different initial conditions (ICs) for the states a and P (shown by white circles) are drawn to show system trajectories starting in different modes. Red arrows have the same IC.

B. Stability

1) Phase Portrait Method: Stability of each of the modes in a hybrid system does not guarantee the stability of the hybrid system [13]. Utilizing phase portraits applied to the nonlinear model, trajectories of a switched system with different initial conditions (IC), P_0 and a_0 , can be tracked and stability can be assessed [13], [14]. Phase portraits of the system regulating about a negative pressure reference (r = -P = -70 kPa), a zero pressure reference (r = 0), and a positive pressure reference $(r = \bar{P} = 169 \text{ kPa})$, were drawn for different ICs, $P_0 = -100:10:300 \text{ kPa}$, and $a_0 = 0:0.05:2 \text{ mm}$. In the case of regulating a negative pressure $r = -\underline{P}$, the trajectories diverge in mode 4 without hybrid control (Fig. 4a), while the hybrid controller causes the trajectories to converge to a limit cycle (Fig. 4b). Marginal stability can also be confirmed for the system with output feedback regulating r = 0 for certain ICs (Fig. 4c, black arrow), while the trajectories realized in the hybrid controller converge to P = 0, $a < a_d$ (Fig. 4d). For $r = \bar{P}$, the trajectories of both the with and without hybrid control systems converge to $P = \bar{P}$, a = 0 (Fig. 4e and f), however, the performance of the system with output feedback is not ideal in Mode 4. These results confirm the stability of the switched system.

2) Multiple Lyapunov-Like Functions (MLF) Method: Given the state space representation in Section II, the developed hybrid system is affine with marginally stable subsystems. As the subsystems are not asymptotically stable, relaxed



Stability analysis using MLF. The system phase portrait, partitions X_1 , X_2 , X_3 , and states values over time are shown (physically infeasible state space is denoted by crosshatches) (a). The trajectories of the system with a negative reference converge to zero pressure and a = 0.5, preventing the system from a loss of pressure feedback, and marginal stability. Lyapunov-like functions value over time for a random initial condition, indicating the stability of the system by meeting Eq. (3)–(5) (b).

conditions and knowledge of the trajectories are required to prove stability of the system via weak Lyapunov-like functions for affine systems [14]-[16]. The hybrid system is stable in the weak sense of Lyapunov when the positive definite Lyapunov-like functions (V_a) associated with the partitions of state space $(X_q, \text{Fig. 1c})$ meet the following relaxed conditions from [15, Th. 3.2]:

$$V_q(x) > 0 \quad for \qquad x \in X_q \tag{3}$$

$$V_q(x) > 0 \quad for \qquad x \in X_q$$

$$V_q(x(t)) \le h(V_q(x(t_q)) \qquad t \in (t_q, t_j)$$
(4)

$$V_q(x(t_{(q,k)})) \le V_q(x(t_{(q,k-1)})) \tag{5}$$

where $h:\mathbb{R}\to\mathbb{R}$ is a continuous function, t_q is the time in which mode q starts and t_j is the time in which mode q ends, and $t_{(q,k)}$ denotes the k^{th} time the system is switched into. To find the Lyapunov-like functions of the form $V_q = \begin{bmatrix} x & 1 \end{bmatrix} \bar{P}_q \begin{bmatrix} x & 1 \end{bmatrix}^T$ associated with each region, the following LMIs [16] are solved for symmetric positive definite P_q

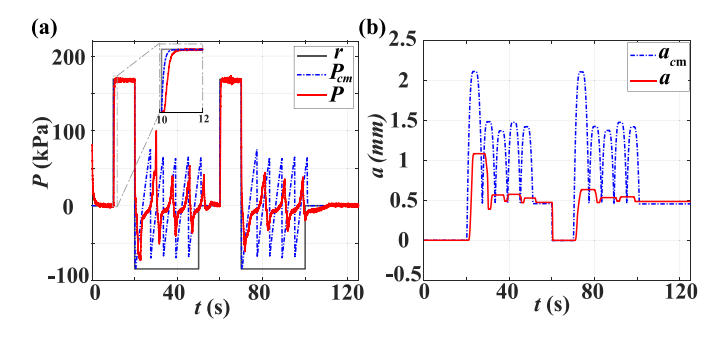


Fig. 6. Implemented hybrid controller is stable in experiments and switches between Modes at the user defined switching surface ($a_d=0.5$ mm). The hybrid control model response, P_{cm} , agrees with the experimental pressure response, P (a). The ink leading edge position in the hybrid control model, a_{cm} , and in the experiment, a (b).

for symmetric U_q and W_q with non-negative entries for each region

$$\begin{cases} \bar{A_q}^T \bar{P_q} + \bar{P_q} \bar{A_q} + \bar{E_q}^T U_q \bar{E_q} \le 0 \\ \bar{P_q} - \bar{E_q}^T W_q \bar{E_q} \ge 0 \end{cases} \quad q \in 1, 2, 3. \tag{6}$$

Given the proposed switching criteria, and that Modes 3 and 4 have the same state matrix, $A_3 = A_4$, and control input, Q_{in} , we divide the physically feasible state space into regions $(X_1, X_2,$ X_3) by defining $\bar{E_1}$, $\bar{E_2}$ and $\bar{E_3}$ (see the Appendix) and solve Eq. (6). Using the linearized system, Eq. (6) was solved and had a feasible solution for P_q . Obtained $V_q s$ (see the Appendix) were numerically checked for Eq. (3)-(5) over a grid space of $P_O = -100:20:100 \ kPa \ \text{and} \ a_O = 0:1:5 \ mm$. In addition, the LMI problem was solved over a grid space of different designs of $\tilde{K} = K/100:10:100K$ and $\tilde{Q}_{in} = \bar{Q}_{in}/100:10:100\bar{Q}_{in}$. Fig. 5a and b show the trajectories and MLF results for a random IC. V_q values are greater than zero (Eq. (3)), are decreasing when a mode is switched-in again (Eq. (4)), and are upper-bounded (Eq. (5)). Eq. (3)-(5) were met for all the ICs, proving the system is stable in the weak sense of Lyapunov. Moreover, the system had a feasible solution for all tested values of \tilde{K} and Q_{in} , proving the system is stable over a wide range of control designs \bar{K} and Q_{in} .

C. Control Scheme Investigation Methods

The designed control scheme was investigated in simulation and experiments. Pulse reference inputs were used for the validations. First, the output feedback control performance for Modes 1 and 2 was tested to see whether it meets the design requirements. Second, the hybrid controller performance, stability, and calculation of the leading edge position was tested in simulation. For experimental investigations, the methods discussed in Section III were utilized. In addition, the time constant during start and stop of the material deposition, and mode transitions were validated.

D. Hybrid Control Implementation Results

Under the output feedback control law, the system achieved the desired time constant $(0.25 \ s)$ as demonstrated in Fig. 6 inset. The experimental control response for the pulse input was in good agreement with the model with a %NRMSE of 7%.

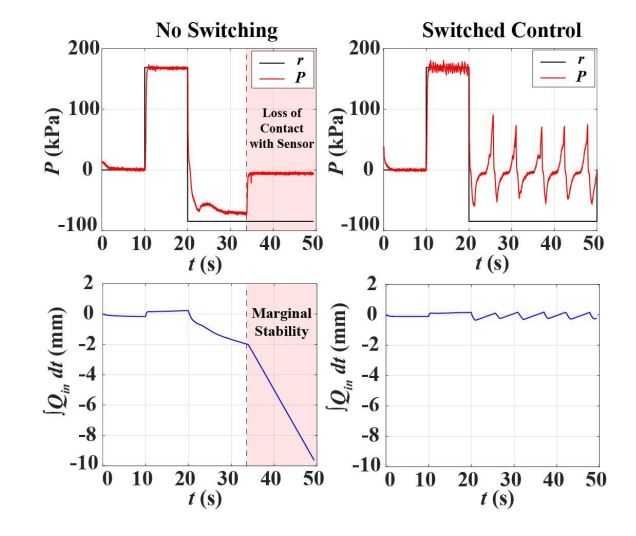


Fig. 7. System response without hybrid control and with hybrid control. The system is marginally stable in mode 4, in the case of no switching. The plunger position keeps decreasing to meet the reference pressure while the measured pressure stays at zero as the feedback is lost.

As it can be observed, at negative reference pressure, the controller switches to Mode 2 in which a is being calculated, and once a passes a_d , which is set to 0.5 mm here, the system switches to Mode 3, where it drives the ink back to a_d and prevents Mode 4, which is the loss of contact with the sensor, from occurring (Fig. 6a). Since the reference signal is still at negative values, the ink will be retracted again, and the controller will fight back until the reference is zero or positive. The model response is in agreement with the experimental data in positive pressures. However, deviations from experimental data are observed in the model response in negative pressures and in the switching instances. Although it is assumed that the system will behave the same in retraction as in extrusion in the model, the actual system behavior is more complicated. In the actual system, slower responses are observed in retraction due to the volume of air that enters into the system and the variable cross-sectional area of the nozzle geometry. This also explains the differences between the ink leading edge (a) calculations in the model and in experiments (Fig. 6b). The implementation of the switched controller prevents the system from becoming marginally stable (Fig. 7). The integration of the input flowrate which is an indicator of plunger position will increase in negative direction indefinitely, as the feedback signal is lost, indicating marginal stability, while in the switched controller the plunger position is bounded and the system is stable.

The controller was tested in a case study, printing lines and shapes that require multiple starts and stops, have multiple corners, and multiple segments with steady-state flowrate regulation. Such structures are of high importance for biomedical applications, such as DW AM of heart valve [17], and intracorporeal DW AM [2], where complex porosity and precision is vital. Here, lines with length of 50 *mm* with start and stop points at certain locations (Fig. 8a), and The Ohio State University logo (Fig. 8c) were chosen to be 3D printed with and without control to demonstrate qualitative improvement of DW AM of parts with the developed controller. The results

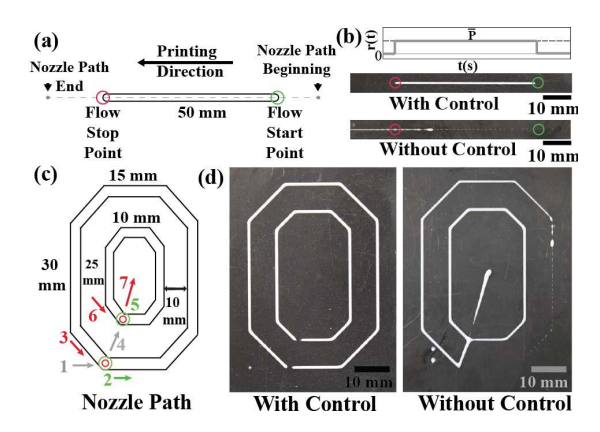


Fig. 8. Case study of printing shapes with and without the implementation of the hybrid controller. Line with the length of 50 *mm* (a) is printed with and without control (b). The Ohio State University logo (c) is printed with and without control (d). The performance of the controller at start and stop of flow rate is considerably improved compared to the no control case.

indicated an appreciable improvement in the shape fidelity of the printed structures with the developed control scheme compared to the without control cases (Figs. 8b and d).

V. CONCLUSION

A hybrid control scheme for the control of ink flowrate in DW AM is designed, analyzed, and implemented. Using output feedback the flowrate can be controlled in Modes 1 and 2, while a predefined open loop control input is designed to control the ink flowrate in Mode 3 and Mode 4. Stability of the hybrid system is assessed using phase portraits and MLF method, demonstrating that the hybrid system is stable. Future directions include the development of more complex control schemes for Mode 2, incorporating the extrusion motor dynamics into the modeling and control, and stability analysis of the system considering different control schemes for Mode 3. The experimental results demonstrated successful flowrate control for printing of parts that require the start and stop of flowrate confirming the performance of the designed hybrid controller.

APPENDIX

In the linearized equations:

$$\begin{split} A_{11} &= -((\frac{1}{2})^{1/n}\beta\pi(\frac{\tau_0}{m})^{1/n}(1-\frac{2L\tau_0}{PR})^{1/n}(48L^3n^3\tau_0)^3\\ &+ 24L^2PRn^2\tau_0^2 + 6LP^2R^2n^2\tau_0 + 6LP^2R^2n\tau_0 + 2P^3R^3n^2\\ &+ 3P^3R^3n + P^3R^3))/(P^4V_r(\frac{L\tau_0}{PR})^{1/n}(6n^3 + 11n^2 + 6n + 1))\\ A_{21} &= -(1/2^{1/n}\pi(\frac{\tau_0}{m})^{1/n}(1-(\frac{2L\tau_0}{PR})^{1/n}(48L^3n^3\tau_0)^3\\ &+ 24L^2PR^2\tau_0^2 + 6LP^2R^2n^2\tau_0 + 6LP^2R^2n\tau_0 + 2P^3R^3n^2\\ &+ 3P^3R^3n + P^3R^3))/(AP^4(\frac{L\tau_0}{PR})^{1/n}(6n^3 + 11n^2 + 6n + 1))\\ B &= \left[\beta/V_r \quad 0\right]^T \end{split}$$

In Section IV, the values of V_q , and h(V) are as follow:

$$\bar{E}_1 = \begin{bmatrix} 0 & 1 & 0 \\ 0 & -1 & 0.5e - 5 \end{bmatrix} \bar{E}_2 = \begin{bmatrix} 0 & 1 & -0.5e - 5 \\ 0 & -1 & 0.5 \end{bmatrix}$$

$$\begin{split} \bar{E}_3 &= \begin{bmatrix} 0 & 0 & 0 \\ 0 & 1 & -0.5 \end{bmatrix} \\ V_1 &= 4.7^{-12}x_1^2 + 2.7^{-20}x_1x_2 + 6.6^{-7}x_1 + 24x_2^2 \\ &\quad + 1.9^{-15}x_2 + 0.023 \\ V_2 &= 4.7^{-12}x_1^2 + 2^{-14}x_1x_2 + 6.6^{-7}x_1 + 1.1^{-7}x_2^2 \\ &\quad + 1.4^{-9}x_2 + 0.023 \\ V_3 &= 4.7^{-12}x_1^2 - 1.3^{-13}x_1x_2 + 7^{-8}x_2^2 \\ &\quad h(V_q(x(t_q)) = 2V_q(x(t_q)). \end{split}$$

ACKNOWLEDGMENT

The authors would like to acknowledge Andrej Simeunovic and Kevin Wolf at OSU for their thoughtful discussions and advice during the production of this letter.

REFERENCES

- [1] T. J. Horn and O. L. A. Harrysson, "Overview of current additive manufacturing technologies and selected applications," *Sci. Progr.*, vol. 95, no. 3, pp. 255–282, 2012.
- [2] A. A. Adib *et al.*, "Direct-write 3D printing and characterization of a GelMA-based biomaterial for intracorporeal tissue engineering," *Biofabrication*, vol. 12, no. 4, Jul. 2020, Art. no. 045006.
- [3] D. J. Hoelzle, S. R. Svientek, A. G. Alleyne, and A. J. W. Johnson, "Design and manufacture of combinatorial calcium phosphate bone scaffolds," *J. Biomech. Eng.*, vol. 133, no. 10, Oct. 2011, Art. no. 101001.
- [4] D. J. Hoelzle, A. G. Alleyne, and A. J. W. Johnson, "Basis task approach to iterative learning control with applications to micro-robotic deposition," *IEEE Trans. Control Syst. Technol.*, vol. 19, no. 5, pp. 1138–1148, Sep. 2011.
- [5] D. J. Hoelzle, A. G. Alleyne, and A. J. W. Johnson, "Iterative learning control for robotic deposition using machine vision," in *Proc. Amer. Control Conf.*, Jun. 2008, pp. 4541–4547.
- [6] A. A. Adib and D. J. Hoelzle, "Hybrid system model of microextrusion-based direct-write additive manufacturing," in *Proc. Amer. Control Conf.*, 2019, pp. 4332–4337.
- [7] R. W. Brockett, "Hybrid models for motion control systems," in *Essays on Control. Progress in Systems and Control Theory*. Boston, MA, USA: Birkhäuser, 1993, pp. 29–53.
- [8] C. Tomlin, G. J. Pappas, and S. Sastry, "Conflict resolution for air traffic management: A study in multiagent hybrid systems," *IEEE Trans. Autom. Control*, vol. 43, no. 4, pp. 509–521, Apr. 1998.
- [9] R. P. Chhabra and J. F. Richardson, Non-Newtonian Flow and Applied Rheology: Engineering Applications. Amsterdam, The Netherlands: Butterworth-Heinemann, Apr. 2011.
- [10] J. P. Hespanha, "Modeling and analysis of networked control systems using stochastic hybrid systems," *Annu. Rev. Control*, vol. 38, no. 2, pp. 155–170, Jan. 2014.
- [11] M. S. Branicky, "Introduction to hybrid systems," in *Handbook of Networked and Embedded Control Systems. Control Engineering*, D. Hristu-Varsakelis and W. S. Levine, Eds. Boston, MA, USA: Birkhäuser, 2005, pp. 91–116.
- [12] A. Simeunović and D. J. Hoelzle, "Nonlinear and linearized gray box models of direct-write printing dynamics," *Rapid Prototyping J.*, vol. 26, no. 10, pp. 1665–1676, 2020.
- [13] D. Liberzon and A. S. Morse, "Basic problems in stability and design of switched systems," *IEEE Control Syst. Mag.*, vol. 19, no. 5, pp. 59–70, Oct. 1999.
- [14] D. Liberzon, Switching in Systems and Control (Systems & Control: Foundations & Applications). Boston, MA, USA: Birkhäuser, 2003.
- [15] R. A. Decarlo, M. S. Branicky, S. Pettersson, and B. Lennartson, "Perspectives and results on the stability and stabilizability of hybrid systems," *Proc. IEEE*, vol. 88, no. 7, pp. 1069–1082, Jul. 2000.
- [16] M. Johansson and A. Rantzer, "Computation of piecewise quadratic Lyapunov functions for hybrid systems," in *Proc. Eur. Control Conf.* (ECC), Jul. 1997, pp. 2005–2010.
- [17] L. A. Hockaday et al., "Rapid 3D printing of anatomically accurate and mechanically heterogeneous aortic valve hydrogel scaffolds," Biofabrication, vol. 4, no. 3, 2012, Art. no. 035005.